








Detection of High-Risk Paraneoplastic Antibodies against TRIM9 and TRIM67 Proteins

Christopher M. Bartley, MD, PhD ^{1,2} Thomas T. Ngo, BS,^{1,2,3} Le Duy Do, PhD,⁴
 Anastasia Zekeridou, MD, PhD  ^{5,6} Ravi Dandekar, BS, MS,^{1,3}
 Sergio Muñiz-Castrillo, MD, PhD ⁴ Bonny D. Alvarenga, BA,^{1,3} Kelsey C. Zorn, BA, MHS,⁷
 Asritha Tubati, BS,^{1,3} Anne-Laurie Pinto, MSc,⁴ Weston D. Browne, BS,^{1,3}
 Patrick W. Hullett, MD, PhD,^{1,3} Mark Terrelonge, MD, MPH,^{1,3} Ryan D. Schubert, MD,^{1,3}
 Amanda L. Piquet, MD,⁸ Binxia Yang, PhD,⁶ Mayra Montalvo, MD,⁵ Andrew F. Kung, BA,⁹
 Sabrina A. Mann, BS,^{7,10} Maulik P. Shah, MD, MHS,^{1,3} Michael D. Geschwind, MD, PhD,^{1,3}
 Jeffrey M. Gelfand, MD, MAS,^{1,3} Joseph L. DeRisi, PhD,^{7,10} Sean J. Pittock, MD ^{5,6}
 Jérôme Honnorat, MD, PhD ⁴ Samuel J. Pleasure, MD, PhD,^{1,3} and
 Michael R. Wilson, MD, MAS ^{1,3}

Objective: Co-occurring anti-tripartite motif-containing protein 9 and 67 autoantibodies (TRIM9/67-IgG) have been reported in only a very few cases of paraneoplastic cerebellar syndrome. The value of these biomarkers and the most sensitive methods of TRIM9/67-IgG detection are not known.

Methods: We performed a retrospective, multicenter study to evaluate the cerebrospinal fluid and serum of candidate TRIM9/67-IgG cases by tissue-based immunofluorescence, peptide phage display immunoprecipitation sequencing, overexpression cell-based assay (CBA), and immunoblot. Cases in which TRIM9/67-IgG was detected by at least 2 assays were considered TRIM9/67-IgG positive.

Results: Among these cases (n = 13), CBA was the most sensitive (100%) and revealed that all cases had TRIM9 and TRIM67 autoantibodies. Of TRIM9/67-IgG cases with available clinical history, a subacute cerebellar syndrome was the most common presentation (n = 7/10), followed by encephalitis (n = 3/10). Of these 10 patients, 70% had comorbid cancer (7/10), 85% of whom (n = 6/7) had confirmed metastatic disease. All evaluable cancer biopsies expressed TRIM9 protein (n = 5/5), whose expression was elevated in the cancerous regions of the tissue in 4 of 5 cases.

View this article online at [wileyonlinelibrary.com](https://onlinelibrary.wiley.com/doi/10.1002/ana.26776). DOI: 10.1002/ana.26776

Received Mar 28, 2023, and in revised form Aug 22, 2023. Accepted for publication Aug 22, 2023.

Address correspondence to Dr Wilson, Weill Institute for Neurosciences, University of California, 675 Nelson Rising Lane, NS212, Box 3206, San Francisco, CA 94158. E-mail: michael.wilson@ucsf.edu; Dr Pleasure, Weill Institute for Neurosciences, University of California, 675 Nelson Rising Lane, NS214, Box 3206, San Francisco, CA 94158. E-mail: samuel.pleasure@ucsf.edu

From the ¹Weill Institute for Neurosciences, University of California, San Francisco, San Francisco, CA, USA; ²Department of Psychiatry and Behavioral Sciences, University of California, San Francisco, San Francisco, CA, USA; ³Department of Neurology, University of California, San Francisco, San Francisco, CA, USA; ⁴French Reference Center on Paraneoplastic Neurological Syndromes and Autoimmune Encephalitis, Hospices Civils de Lyon and SynatAc Team, Institut Mécanismes in Integrated Life Sciences, L'Institut national de la santé et de la recherche médicale, U1314/CNRS UMR 5284, Universités de Lyon, Université Claude Bernard Lyon 1, Lyon, France; ⁵Department of Neurology, Center for Multiple Sclerosis and Autoimmune Neurology, Mayo Clinic, Rochester, MN, USA; ⁶Department of Laboratory Medicine and Pathology, Mayo Clinic, Rochester, MN, USA; ⁷Department of Biochemistry and Biophysics, University of California, San Francisco, San Francisco, CA, USA; ⁸Department of Neurology, University of Colorado Anschutz Medical Campus, School of Medicine, Aurora, CO, USA; ⁹PhD Degree Program in Biological and Medical Informatics, School of Medicine, University of California, San Francisco, San Francisco, CA, USA; and ¹⁰Chan Zuckerberg Biohub, San Francisco, CA, USA

Additional supporting information can be found in the online version of this article.

1086 © 2023 The Authors. *Annals of Neurology* published by Wiley Periodicals LLC on behalf of American Neurological Association. This is an open access article under the terms of the [Creative Commons Attribution-NonCommercial-NoDerivs](https://creativecommons.org/licenses/by-nc-nd/4.0/) License, which permits use and distribution in any medium, provided the original work is properly cited, the use is non-commercial and no modifications or adaptations are made.

Interpretation: TRIM9/67-IgG is a rare but likely high-risk paraneoplastic biomarker for which CBA appears to be the most sensitive diagnostic assay.

ANN NEUROL 2023;94:1086–1101

Co-occurring TRIM9/67 autoantibodies (TRIM9/67-IgG) are proposed paraneoplastic biomarkers that are associated with a subacute cerebellar syndrome, typically in the setting of lung cancer.^{1–3} Importantly, TRIM9/67-IgG has not been detected in the sera or cerebrospinal fluid (CSF) of small cell lung cancer (SCLC) patients without a paraneoplastic neurological syndrome (PNS), autoimmune encephalitis patients, or patients with noninflammatory neurodegenerative disorders.¹ Therefore, TRIM9/67-IgG is not a general marker of cancer or neural injury. However, because only very few cases have been reported, the best detection method for TRIM9/67-IgG is unknown, and its usefulness as a paraneoplastic biomarker has not been definitively established.

Here, we evaluated biospecimens from candidate TRIM9/67-IgG identified across 3 institutions by rodent brain tissue-based assay, immunoblot, overexpression cell-based assay (CBA), and panhuman proteome phage display immunoprecipitation sequencing (PhIP-Seq).^{3,4} The 13 cases that were positive for TRIM9/67 antibodies by at least 2 methods were considered TRIM9/67-IgG positive. We reviewed these patients' medical histories and characterized available tumors from 5 of the TRIM9/67-IgG cases.

Patients and Methods

Human Subjects

Written informed consent was obtained from subjects or a surrogate (University of California, San Francisco [UCSF] Institutional Review Board [IRB] 13-12;236). Additional subjects were enrolled through the Mayo Clinic Neuroimmunology Laboratory (IRB 08-007810) and the NeuroBioTec Biobank (Hospices Civils de Lyon Biological Resource Center, France, AC-2013-1867, NFS96-900, GenePNS, 19-62, NCT-03963700).

Evaluation of Specificity of Anti-TRIM9 and Anti-TRIM67 Antibodies Used for Murine and Human Tissue-Based Immunofluorescence and Immunohistochemistry

Because TRIM67 is a paralog of TRIM9 that arose through genome duplication,⁵ there is a risk of commercial antibody cross-reactivity. Therefore, we evaluated the specificity of the anti-TRIM9 (MyBioSource, San Diego, CA; MBS9603565, 1:100)^{6,7} and anti-TRIM67 (Proteintech, Rosemont, IL; 24,369-1-AP, 1:25) antibodies that were used for mouse brain and tumor immunohistochemistry

(IHC) by TRIM9-FLAG and TRIM67-FLAG overexpression CBAs. Monoclonal anti-FLAG M2 antibody (Sigma-Aldrich, St Louis, MO; F1804) was used at 1:1,000 to detect FLAG.

Whereas the anti-TRIM67 antibody was specific to TRIM67, anti-TRIM9 was immunoreactive to both TRIM9 and TRIM67 (data not shown). However, TRIM9 and TRIM67 exhibited different subcellular distributions in HEK293T cells and mouse brain, and TRIM9 expression generally did not overlap with TRIM67 in brain tissue. Moreover, the immunostaining patterns for TRIM9 and TRIM67 mirrored cell type-specific gene expression patterns of TRIM9 and TRIM67 in the murine cerebellum.⁸

Cell-Based Assays

To validate TRIM9/67 autoantibodies in CSF and sera, HEK 293 cells were transfected with pCS2-*TRIM9* plasmid (encoding N-terminal myc-tagged human TRIM9) or pCS2-*Trim67* plasmid⁹ (encoding murine N-terminal myc-tagged Trim67). Fixed and permeabilized cells were immunostained with patient CSF (1:10) or serum (1:100) and a commercial rabbit monoclonal anti-Myc antibody (Sigma-Aldrich; C3956), and counterstained with the appropriate fluorochrome-conjugated secondary antibodies at 1:1,000 (Fisher Scientific, Waltham, MA; A21433 and A11034). CBAs were blindly read by 3 independent raters using an Ni-U fluorescent microscope (Nikon, Champigny-sur-Marne, France).

For B-box 2 domain CBAs, HEK293 T cells were plated onto 10mm poly-d-lysine-coated (50µg/ml) coverslips in 24-well plates. Cells were transfected overnight using Lipofectamine 3000 with either pCMV6-hTRIM9-Myc-DDK (Origene, Rockville, MD), pCS2-hTRIM67-C-FLAG (Lyon), or pcDNA3.1(+)-C-DYK plasmids encoding amino acids 217–256 of human TRIM9 or amino acids 303–361 of human TRIM67 (Genscript, Piscataway, NJ). Transfected cells were rinsed with ice cold 1 × phosphate-buffered saline (PBS) the following day, then fixed with 4% paraformaldehyde for 10 minutes. Fixed cells were rinsed with PBS several times, then blocked and permeabilized for 30 minutes with 5% lamb serum in PBS containing 0.5% Triton X-100.

To screen for B-box 2 immunoreactivity, transfected cells were stained with anti-FLAG antibody at 1:1,000 and CSF at 1:10 in 5% blocking buffer overnight at 4°C. Cells were rinsed with PBS 4 times, then stained with Alexa Fluor secondaries at a 1:1,000 dilution in 5% blocking buffer. Nuclei were stained with 4,6-diamidino-

2-phenylindole (DAPI) at 1 μ g/ml in PBS for 5 minutes. Stained slides were then mounted onto microscope slides with Prolong Gold antifade.

Animal Subjects

Tissue from postnatal day 40–60 mice was used for immunostaining, immunoprecipitations, and immunoblotting (Jackson Laboratory, Bar Harbor, ME; F1 cross of FVB [cat. #001800] \times C57BL/6J [cat. #000664]). Slides for indirect immunofluorescence on mouse tissue (brain, gut, kidney) were acquired (Scimedx, Denville, NJ). Animal procedures complied with federal guidelines and the institutional policies of the UCSF Institutional Animal Care (AN183338-02B) or Use Committee and the French Ethical Committee of the Lyon 1 University (DR2013-47) in accordance with European Community Council directive 2010/63/EU.

Rodent Brain Tissue-Based Immunofluorescence

At UCSF, mouse tissue was prepared as previously described¹⁰ and incubated overnight with or without anti-TRIM9 or anti-TRIM67 antibodies at 4°C prior to secondary immunostaining and imaging using a Zeiss (Oberkochen, Germany) Axio Scan Z.1 Slide Scanner and Nikon CSU-W1 spinning disk confocal microscope followed by image preparation with ImageJ (version 2.1.0/1.53c).

At Mayo, specimens were tested on murine tissue cryosections as previously described¹¹ at screening dilutions of 1:240 for serum (preabsorbed with liver powder) or 1:2 for CSF.

At Lyon, freshly prepared adult rat brains were prepared as previously described¹ (but using 12 μ m-thick sections) prior to immunostaining with CSF (1:10) and imaging on a Zeiss Axio Scan.Z1.

Tumor Histology, IHC, and Multiplex Immunofluorescence

Hematoxylin and eosin slides were prepared in Leica (Wetzlar, Germany) Autostainer XL; slides stained in hematoxylin (Thermo Fisher Scientific, Waltham, MA; Shandon Instant Hematoxylin, cat. #6765015) for 7 minutes and in eosin (Thermo Fisher Scientific, Shandon Instant Eosin-Y Alcoholic, cat. #531946) for 20 seconds.

Multiplex immunofluorescence staining was performed on the Ventana BenchMark Ultra using Discovery reagents (Ventana Medical Systems, Tucson, AZ) according to manufacturer's instructions, except as noted. Heat induced epitope retrieval was performed with the Cell Conditioning 1 solution (cat. #950-124) for 32 minutes at 97°C. Primary antibodies used were TRIM9 (1:100, MBS710195), TRIM67 (1:25, 24,369-1-AP), estrogen receptor (ER; SP1; Abcam, Cambridge, MA; ab1660,

1:50), and pancytokeratin (panCK; 1:100, KRT/1877R, ab234297). The primary antibodies were detected with Discovery Red 610 Kit (cat. #760-245), FAM Kit (cat. #760-243), and Cy5 Kit (cat. #760-238) respectively. Finally, slides were counterstained with DAPI (Akoya Biosciences, Menlo Park, CA, cat. #FP1490).

PhIP-Seq Protocol and Analysis

PhIP-Seq uses patient IgG to immunoprecipitate T7 bacteriophages that display 49 amino acid human peptides on their viral capsid. PhIP-seq was performed as previously described using two rounds of enrichment.⁴

To evaluate for TRIM9 and TRIM67 enrichment at the whole protein level, for each sample individual scaled peptide read counts (reads per 100,000 [rpK]) were summed for TRIM9 and TRIM67. The *Z* score of the summed rpK for each protein for each sample relative to healthy control samples was calculated. A *Z* score ≥ 3 was interpreted as significantly enriched.

Chemiluminescent Immunoblot

Whole adult rat brains were first dissected. The tissue was then homogenized in lysis buffer containing 50mM Tris-HCl pH 7.5, 150mM NaCl, 1mM ethylenediaminetetraacetic acid, 1% NP-40, 0.5% deoxycholate, 0.1% sodium dodecyl sulfate (SDS), orthovanadate, benzamide phosphatase inhibitor, and protease inhibitor. The homogenate was incubated on ice for 30 minutes and sonicated. Cell debris was discarded by 20-minute centrifugation at 16,000 $\times g$ and 4°C. Then, 10 μ g of whole brain protein extract was used for Western blotting to screen for bands recognized by patient CSF (1:100).

Immunoprecipitation Mass Spectrometry

Immunoprecipitation mass spectrometry (IP-MS) was performed as previously described.¹⁰ Analysis was limited to spectral counting using Scaffold version 4.

Results

Clinical Phenotypes of TRIM9/67-IgG-Positive Cases

Clinical history for TRIM9/67-IgG cases was available for 10 of 13 cases as summarized in the Table S1 and Supplemental Case Histories.

Cerebellar Syndrome

Seven of 10 (Cases 1–6 and 10) presented with subacute cerebellar syndrome, 3 of which (Cases 2–4) were previously published.^{1,2} All cerebellar syndrome cases developed a pancerebellar syndrome over 3 to 4 weeks. Additional features were noted in Case 1, who developed cerebellar cognitive affective syndrome, and in

Case 3, who developed dysexecutive symptoms and anterograde amnesia.

Six of the 7 cerebellar syndrome patients had cancer: lung adenocarcinoma ($n = 3$), SCLC ($n = 1$), melanoma ($n = 1$), and breast cancer ($n = 1$). Four developed the cerebellar syndrome after their cancer diagnosis. Among them, 2 (Cases 1 and 2) developed the cerebellar syndrome after their second and fourth cycle of immune checkpoint inhibitor therapy, respectively. In the remaining 2 cases, the malignancy was found during workup for a PNS. All 6 cancer patients had metastatic disease at the time of their neurological presentation.

Acute phase CSF testing revealed a mild to moderate lymphocytic pleocytosis in all cerebellar syndrome cases (8–74 cells/ μ l, reference ≤ 5 cells/ μ l), whereas total protein was normal or modestly elevated (elevated in $n = 3$, 58–98mg/dl, reference ≤ 50 mg/dl). All 4 cases with available results had an elevated IgG index, 3 of whom also had CSF-restricted oligoclonal bands (OCBs). Commercial antineural autoantibody testing was negative in all cases. Only 1 of the 6 cases treated with at least 1 immunomodulatory agent showed improvement in neurologic symptoms (Table S1).

Encephalitis

Of the 3 remaining cases with available clinical history (Cases 7–9), 2 (Cases 7 and 8) presented with subacute limbic encephalitis and 1 with subacute possible autoimmune encephalitis according to diagnostic criteria (Case 9).¹²

Two of 3 encephalitis patients (Cases 7 and 8) had a mild lymphocytic pleocytosis (16 and 6 cells/ μ l, respectively), had an elevated IgG index (1.9 and 1.1, respectively), and >5 CSF-restricted OCBs (Case 9 was not tested for OCBs). Although initially negative for known ant-ineural autoantibodies, Case 7 developed serum acetylcholine receptor antibodies and myasthenia gravis 1 year later (thymoma was not detected by chest computed tomography [CT]). Case 8 had high-titer GAD65 antibodies in the serum (1,389nmol/l, reference ≤ 0.02) and CSF (36.4nmol/l, reference ≤ 0.02).

Case 7 had notable improvement of attention, awareness, and cognitive processing after treatment with levetiracetam, high-dose oral prednisone, and multiple rounds of plasmapheresis but within the next year suffered a subacute decline in mental status and a recurrence of seizures. He had several body CT and positron emission tomography scans without evidence of a tumor. Despite multiple immunotherapies, he continued to decline and passed away approximately 3.5 years after disease onset. No autopsy was performed. Case 8 initially responded to antiepileptic medications, but her GAD65 antibodies persisted during convalescence (serum, 1,983nmol/l), and her

seizures became medically refractory despite glucocorticoids and rituximab. Case 9 experienced a near complete resolution of memory impairment after a combination of chemotherapy and immunosuppression.

Molecular Characterization of TRIM9/67-IgG Cases

Summary results across all assays are provided in Figure 1.

Tissue-Based Immunofluorescence in the Murine Brain

TRIM9/67-IgG cases were less common than anti-Yo (6 vs 91) and similar to anti-Ri (6 vs 7) when comparing relative frequencies over a single year in the Mayo Clinic Neuroimmunology database ($N = 98,984$ samples tested by tissue-based immunofluorescence [TBIF] in 2020). Similarly, at Hôpital Neurologique in 2020, only 1 patient was positive for TRIM9/67-IgG compared to 15 anti-Yo and 7 anti-Ri patients ($N = 16,910$ tested on TBIF). All candidate TRIM9/67 cases were identified by rodent brain tissue staining except Cases 7 and 8, which were initially identified by PhIP-Seq. Every case but Case 8 produced characteristic widespread immunostaining of neuronal somata in the olfactory bulb, cortex, hippocampus, thalamus, and molecular and Purkinje cell layers of the cerebellum (Fig 2A).¹ In contrast, Case 8 CSF produced a GAD65-like immunostaining pattern, consistent with the patient's known GAD65-IgG positivity.

Using CSF from a representative case (Case 1), we found that patient IgG colocalized with anti-TRIM9 in all anatomic regions (see Fig 2B). In contrast, cerebellar TRIM67 protein expression was nearly undetectable by TBIF, consistent with 6-fold lower cerebellar TRIM67 than cerebellar TRIM9 gene expression according to ProteinAtlas.org¹³ (see Fig 2C).

Detection of TRIM9/67-IgG by HEK293 Cell-Based Overexpression Assay

By CBA, CSF and/or sera from all 13 cases were positive for TRIM9/67-IgG (Fig 3). By end-point dilution series, there was no overall difference between anti-TRIM9 and anti-TRIM67 antibody titers ($p = 0.45$, paired Wilcoxon rank test). However, CSF TRIM9-IgG and TRIM67-IgG titers were lower in encephalitis cases than cerebellar syndrome cases ($p = 0.0317$ and $p = 0.0159$, respectively), but there was no difference in serum titers, nor was there a difference in titers between cases of unknown phenotype and cerebellar cases. TRIM9 and TRIM67 antibody titers were significantly higher in serum than in CSF ($p = 0.002$ for both TRIM9 and TRIM67). Nonetheless, within samples, TRIM9 and TRIM67 antibody titers were well correlated ($r^2 = 0.78$).

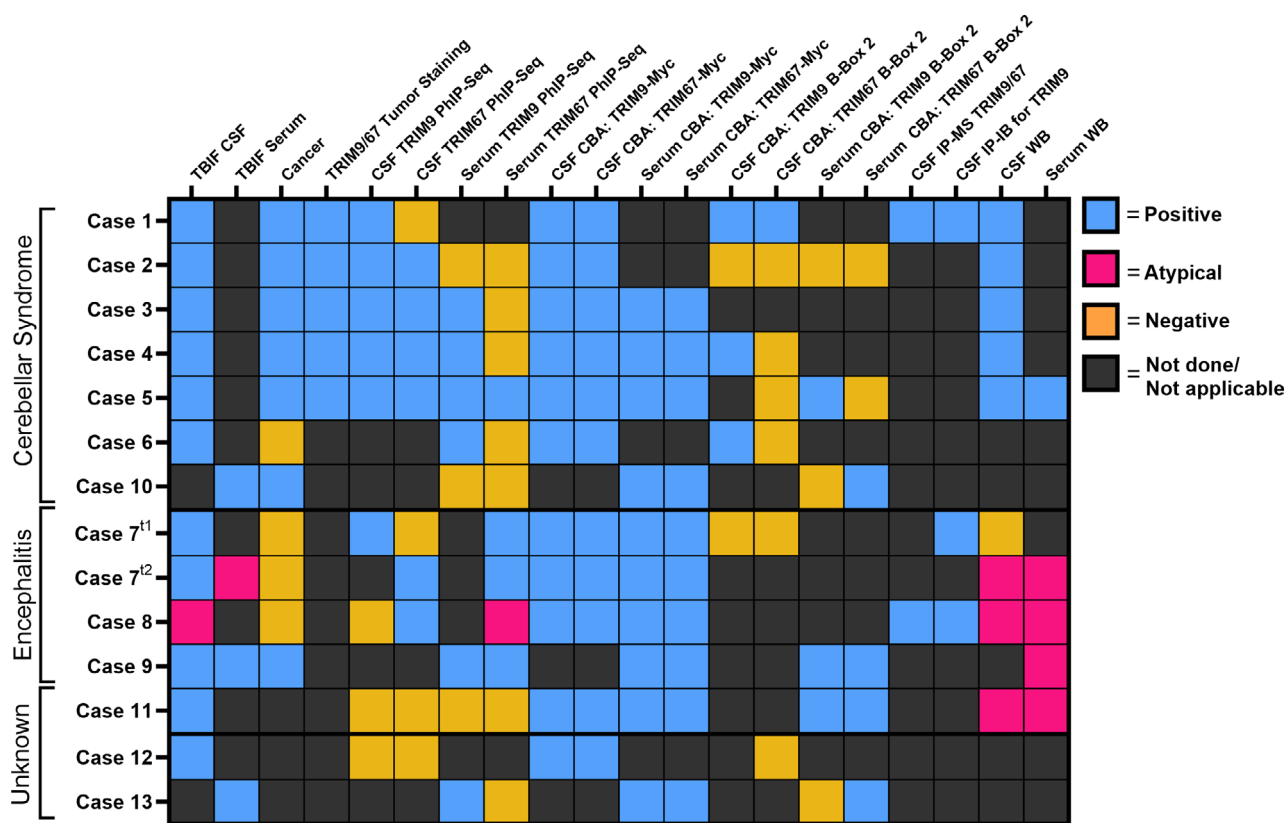


FIGURE 1: Cases, biospecimens, and outcomes for each assay. Categorical heatmap shows cases, assays, and assay results. CBA = cell-based assay; CSF = cerebrospinal fluid; IP-IB = immunoprecipitation followed by immunoblot; IP-MS = immunoprecipitation mass spectrometry; PhIP-Seq = phage display immunoprecipitation sequencing; t1 = time point 1; t2 = time point 2; TBIF = tissue-based immunofluorescence; WB = Western blot. [Color figure can be viewed at www.annalsofneurology.org]

Detection of TRIM9/67-IgG by Immunoblot

Mass spectrometry previously demonstrated that TRIM9 and TRIM67 are present at 95kDa, whereas only TRIM9 is present at 72kDa.¹ Therefore, we tested whether immunoblot is as sensitive as CBA. Cases 2, 3, and 4 were previously shown to recognize the 95 and 72kDa bands.^{1,2} CSF from newly reported Cases 1 and 5 primarily recognized the 95 and 72kDa bands, whereas Cases 9 and 11 recognized TRIM9/67 and additional bands, suggesting the presence of other antineural antibodies. In contrast, Cases 7 and 8 both produced a lower band of approximately 60kDa but no bands at the expected molecular weights (see Fig 3E).

Detection and Characterization of TRIM9/67-IgG by PhIP-Seq

We evaluated the sensitivity of PhIP-Seq^{4,14} for TRIM9/67 antibodies at the protein and peptide levels. At the protein level, 11 of 18 and 7 of 18 biospecimens enriched TRIM9 and TRIM67, respectively (Fig 4). At the peptide level, 17 and 16 of 18 biospecimens enriched at least 1 TRIM9 or TRIM67 peptide, respectively. The dominant peptide for both TRIM9 and TRIM67 mapped

to the homologous B-box type 2 (B-box 2) domain, a zinc-finger domain of unknown function. The B-box 2 epitopes are predicted to be conformational, and cases that enriched the B-box 2 peptide by PhIP-Seq were positive by TRIM9 or TRIM67 B-box 2 domains by CBA (see Figs 1 and 4D), but overall, B-box 2 CBA was less sensitive than whole protein CBA. Curiously, despite their homology, TRIM9 and TRIM67 B-box 2 domains exhibited different subcellular localization.

The finding that some cases were immunoreactive to TRIM9 and TRIM67 by CBA but not denaturing immunoblot suggests that some TRIM9/67 autoantibodies bind to conformational epitopes. However, B-box 2 expression levels were too low to test for loss of autoantibody binding following denaturing SDS-polyacrylamide gel electrophoresis. Therefore, we assessed for conformational epitope-dependent TRIM9/67 autoantibodies by immunoprecipitation. We immunoprecipitated mouse brain tissue lysate with CSF from Case 8, which failed to enrich or bind to TRIM9 by PhIP-Seq and immunoblot, respectively. Like Cases 1 and 7, which did enrich TRIM9 by PhIP-Seq, Case 8 immunoprecipitated the 3 major TRIM9 isoforms (see Fig 4E). Likewise, Case 7 robustly immunoprecipitated TRIM9 and TRIM67 as

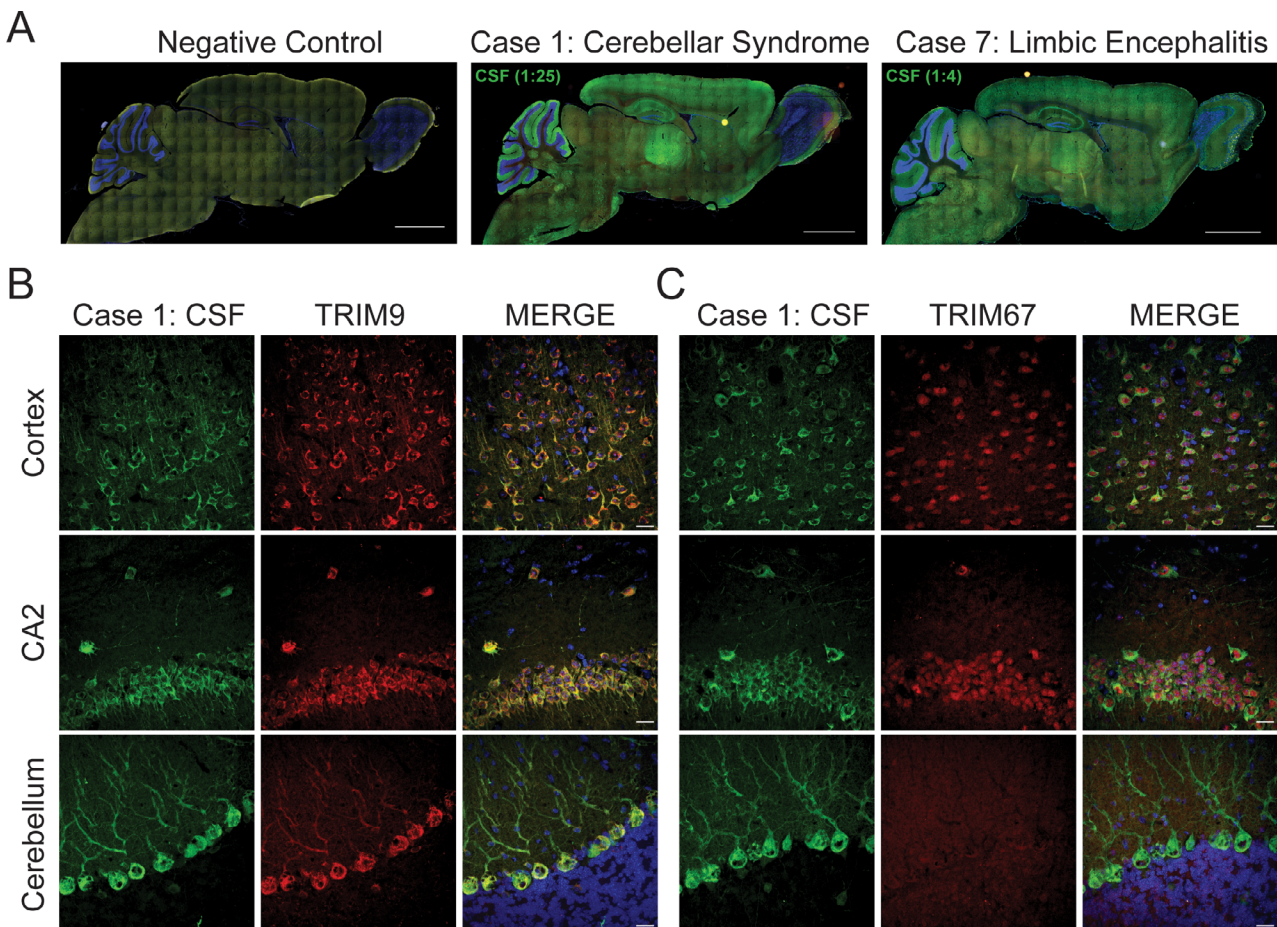


FIGURE 2: Tissue-based immunofluorescent assays. (A) Panoramic images of cerebrospinal fluid (CSF) IgG (green) from 2 representative TRIM9/67 cases. Case 1 was immunostained at a 1:25 CSF dilution and Case 7 at a 1:4 dilution. Nuclei are stained with 4,6-diamidino-2-phenylindole (blue). Scale bars = 2mm. (B) Coimmunostaining of Case 1 CSF (green), TRIM9 (red), and nuclei (blue) in the cortex, CA2 of the hippocampus, and cerebellum. Scale bars = 20µm. (C) Coimmunostaining of Case 1 CSF (green), TRIM67 (red), and nuclei (blue) in the cortex, CA2 of the hippocampus, and cerebellum without antigen retrieval. Scale bars = 20µm. [Color figure can be viewed at www.annalsofneurology.org]

determined by IP-MS despite not enriching TRIM67 by PhIP-Seq (see Fig 4F).

To further characterize the autoantibody profile of TRIM9/67 syndromes, we expanded our PhIP-Seq analysis to the entire human proteome. To be conservative, we used a previously described analytic approach that looks for sets of overlapping peptides enriched at least 10-fold above controls whereby at least 1 peptide in the set is enriched at least 100-fold.^{10,15} We then compared these candidates to a database of 4,206 healthy serum, healthy CSF, and negative control (bead only) PhIP-Seq runs.

We found that Case 9, who had encephalitis and SCLC, enriched ZIC1, a paraneoplastic autoantigen associated with SCLC and paraneoplastic cerebellar degeneration.¹⁶ Previously classified autoantigens were not enriched by other cases. However, Case 5 enriched peptides mapping to the B-box type 1 domain of TRIM1 (also known as MID2) and TRIM9, suggesting that anti-TRIM9/67 autoantibodies may cross-react with other TRIM family proteins.

We next considered whether TRIM9/67 antibodies might be incidental to a distinct encephalitis syndrome. However, we failed to find a shared alternate candidate autoantigen among encephalitis cases by PhIP-Seq. Nonetheless, we identified candidate autoantigens with putative relevance, including SIPA1L1, which may regulate seizure threshold¹⁷ (Case 8), and astrocyte-enriched PHF21B, which has been implicated in SCLC¹⁸ (Case 9). Case 7 also enriched peptides to RTP5, an uncharacterized protein that is highly expressed in the hypothalamus.¹³

Immunohistochemistry of TRIM9 and TRIM67 in the Human Brain

Anatomic characterization of TRIM9 and TRIM67 protein expression in the human brain is limited.^{6,19} We found human cerebellar TRIM9 expression largely mirrored expression in the murine cerebellum and was characterized by strong immunoreactivity of Purkinje cell bodies, primary and secondary Purkinje cell dendrites, and

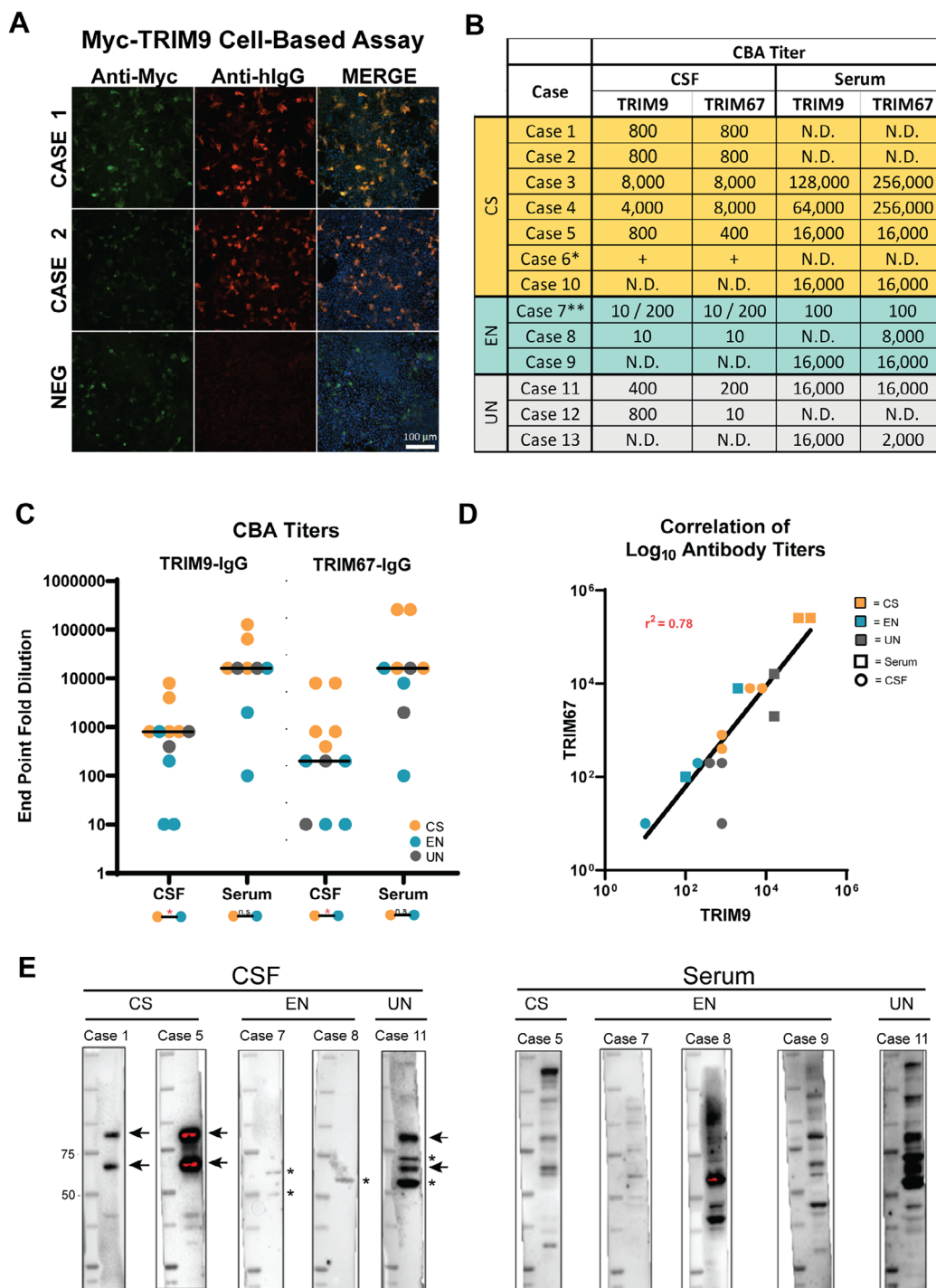
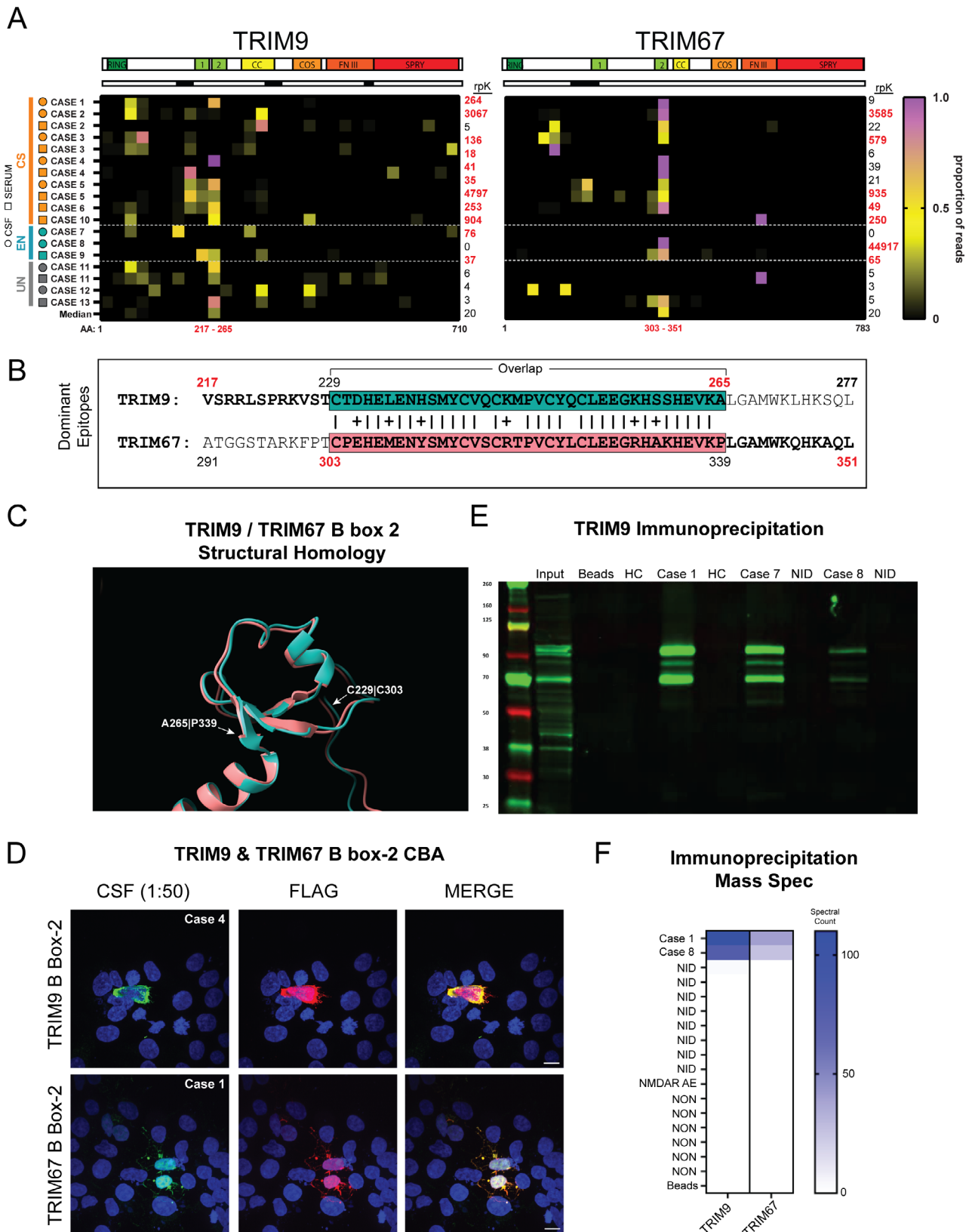


FIGURE 3: Validation of TRIM9/67-IgG by cell-based assay (CBA) and immunoblot. (A) HEK 293 T cells were transfected with myc-TRIM9 or myc-Trim67 and immunostained with anti-Myc (green), patient cerebrospinal fluid (CSF) or serum (anti-human IgG, red), and 4,6-diamidino-2-phenylindole nuclear counterstain (blue). CSF CBAs (1:10 dilution) from 2 representative cases are shown. Scale bar = 100 μ m. NEG = negative. **(B)** Table of CBA end point titers. *Case 6 was positive by CBA, but there was insufficient CSF to complete the dilution series. **Two time points were tested for Case 7 CSF (earlier time point to the left of the slash). CS = cerebellar syndrome; EN = encephalitis; N.D. = not done; UN = unknown phenotype. **(C)** Dot plots of TRIM9 and TRIM67 autoantibody titers as determined by end-point dilution CBAs. Unbroken line = median titer. Barbells below each data column indicate whether there is a significant (* $p < 0.05$) or nonsignificant (n.s.) difference between autoimmune EN and CS cases as determined by 2-tailed unpaired Mann-Whitney tests. **(D)** Log scale scatterplot of within-sample TRIM9:TRIM67 autoantibody titer as determined by CBA; r^2 was determined by simple linear regression. **(E)** Immunoblots of whole rat brain lysate with CSF and serum. Cases 1 and 5 show the typical banding pattern at 72kDa and 95kDa. Cases 7, 8, 9, and 11 show atypical banding patterns as indicated by the asterisks. Black arrows = TRIM9/67 bands. Asterisks = unexpected bands. [Color figure can be viewed at www.annalsofneurology.org]



(Figure legend continues on next page.)

light staining of the molecular layer neuropil. In contrast, TRIM67 immunostaining was scarcely detected in Purkinje cells, whereas strong nuclear immunoreactivity

was observed in granule cells and interneurons in the molecular layer (Fig 5). In human temporal lobe, subtle differences between TRIM9 and TRIM67 protein

expression were appreciated. TRIM9 staining was stronger in the outer layers of the temporal lobe relative to deeper layers. In general, in both the entorhinal cortex and hippocampus, the regional expression of TRIM9 and TRIM67 was generally complementary (the inverse of each other) and did not overlap (see Fig 5).

TRIM9/67 Protein Expression in Patient Cancer

We performed IHC on benign tissue, primary melanoma, and metastatic melanoma from Case 1. TRIM9 colocalized with metastatic but not primary melanocytic cells or benign cells. In contrast, TRIM67 did not preferentially colocalize with either primary or metastatic melanoma cells (Fig 6A–C).

We assessed tumors from 4 additional TRIM9/67-IgG patients (Cases 2–5). Biopsies from Cases 2 to 4 expressed the tumor marker panCK. Similar to Case 1, metastatic SCLC tissue from Case 2 had significantly higher anti-TRIM9 immunofluorescence in panCK^{high} than panCK^{low} regions. In contrast, TRIM67 immunofluorescence did not differ between panCK^{high} and panCK^{low} regions. In primary and metastatic lung adenocarcinoma from Case 3, both TRIM9 and TRIM67 immunofluorescence was significantly higher in panCK^{high} than panCK^{low} regions. Finally, in primary lung adenocarcinoma from Case 4, the relationship between TRIM9 and TRIM67 and panCK varied by cytoarchitecture. TRIM9 and TRIM67 signals were significantly higher in disorganized clusters of panCK^{high} cells, but unchanged in regions where panCK^{high} cells were organized in epithelial or glandularlike arrangements (see Fig 6D,E). In Case 5's ER+ primary and metastatic breast cancer biopsies, we detected qualitatively similar TRIM9 protein expression in ER+ and ER– regions. In contrast to TRIM9, TRIM67

expression was qualitatively lower in ER– regions than ER+ regions (Fig 7).

Discussion

Anti-Yo, -DNER, -KLHL11, and -Ri are well-characterized autoantibody biomarkers of paraneoplastic cerebellar degeneration (PCD). However, more than two thirds of known paraneoplastic autoantibodies with frequent (>50%) cerebellar involvement are poorly characterized owing to small case numbers, including TRIM9/67-IgG.²⁰ Here, we performed an extensive search for additional TRIM9/67-IgG cases and confirmed their rarity relative to anti-Yo and anti-Ri antibodies. These additional cases have allowed us to characterize this rare disease more extensively.

Importantly, this expanded TRIM9/67-IgG cohort allowed us to determine that whole protein CBA appears to be the most sensitive TRIM9/67-IgG detection method, with TRIM9 and TRIM67 CBAs being equally sensitive. Of our 13 cases, 10 had available clinical history, and 7 of these had cancer, including the second reported case of TRIM9/67-IgG cerebellar syndrome following checkpoint inhibitor therapy (Case 1). In addition, Case 5 had breast cancer, a new TRIM9/67-IgG cancer association. This expanded cohort indicates that TRIM9/67-IgG are likely high-risk, albeit rare, paraneoplastic autoantibodies that should be included in routine paraneoplastic autoantibody testing.²¹ More conservatively, if those cases without available clinical information did not have cancer, the TRIM9/67-IgG cancer association drops to 54%, which would place TRIM9/67-IgG in the category of intermediate risk paraneoplastic biomarkers.

This study has revealed that TRIM9/67-IgG cerebellar syndrome is similar to well-characterized PCD associated with intracellular onconeural antigens in many respects.

FIGURE 4: TRIM9/67-IgG epitope mapping. (A) Top, linear TRIM9 and TRIM67 protein structures. Protein domains align to peptides in heatmaps below. The white and black band beneath TRIM9 and TRIM67 protein structures denotes peptides (black) enriched by a TRIM9/67-IgG-positive individual from a prior study.³ Heatmaps are colored according to the proportion of phage display immunoprecipitation sequencing reads that map to individually enriched peptides. Total reads per 100,000 (rpK) for TRIM9 and TRIM67 are shown to the left of each heatmap; bolded red = rpK significantly greater than controls (Z score ≥ 3), black = rpK not significant. CS = cerebellar syndrome; CSF = cerebrospinal fluid; EN = encephalitis; UN = unknown phenotype. The bottom row represents the median enrichment of each peptide across all samples. The red numbers indicate the N and C terminal amino acid (AA) positions for the dominant TRIM9 (Uniprot ID #Q9C026, isoform 1) and dominant TRIM67 (Uniprot ID #Q6ZTA4, isoform 1) peptide. (B) Sequences of the dominant TRIM9 and TRIM67 peptides. The bolded letters between indicated AAs encode target peptides demarcated by red numbers below the heatmap in A. Vertical lines indicate identical AAs in the overlapping region between the dominant TRIM9 and TRIM67 peptide, plus signs indicate chemically similar AAs, and gaps indicate dissimilar AAs. The overlapping sequence is shown in teal (TRIM9) and salmon (TRIM67). (C) AlphaFold models were imported into ChimeraX, and the B-box 2 domain of TRIM67 (salmon) was aligned to the B-box 2 domain of TRIM9 (teal). (D) TRIM9 and TRIM67 B-box 2-FLAG overexpression cell-based assays (CBAs). The top row shows Case 4 CSF (green) binding to cytoplasmic FLAG-tagged TRIM9 B-box2 (red). The bottom row demonstrates Case 1 CSF (green) binding to FLAG-tagged TRIM67 B-box-2 (Red). (E) Immunofluorescent immunoblot following immunoprecipitation of TRIM9 from mouse brain lysate without CSF (beads) or with CSF from Cases 1, 7, and 8, healthy controls (HC; n = 2), or other neuroinflammatory cases (NID; n = 2). (F) Heatmaps of spectral counts of TRIM9 and TRIM67 peptide identified by mass spectrometry after immunoprecipitation without CSF (beads), or with CSF from Cases 1 and 8, other neuroinflammatory disorders (NID; n = 8), or noninflammatory CSF samples (n = 6). AE = autoimmune encephalitis, CC = GST-coiled coil domain, COS = C-terminal subgroup one signature, FN = fibronectin, NMDAR = N-methyl-D-aspartate receptor, SPRY = SPlA/ryanodine receptor domain [Color figure can be viewed at www.annalsofneurology.org]

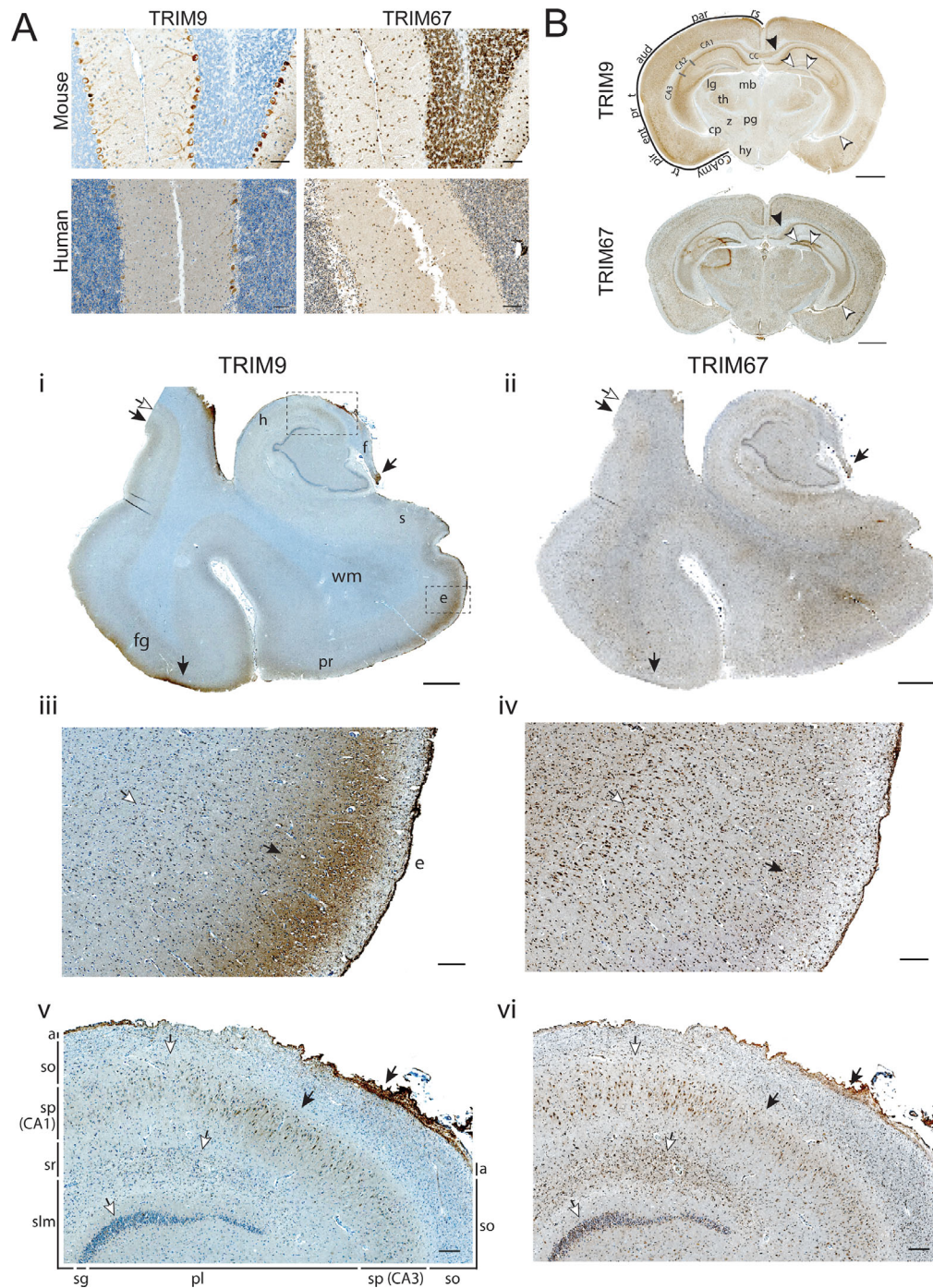


FIGURE 5: Immunohistochemistry (IHC) of TRIM9 and TRIM67 in the murine and human brain. (A) 3,3'-Diaminobenzidine (DAB) immunostaining of mouse and human formalin-fixed, paraffin-embedded cerebellum. Mouse scale bars = 50 μ m. Human scale bars = 100 μ m. (B) DAB immunostaining of serial coronal adult mouse brain sections. Anatomic annotations: aud = auditory cortex; cc = corpus callosum; CoAmy = cortical amygdalar layer; cp = cerebral peduncle; ent = entorhinal cortex; hy = hypothalamus; lg = lateral geniculate; mb = midbrain; par = parietal cortex; pg = periaqueductal grey; pir = piriform cortex; pr = perirhinal cortex; rs = retrosplenial cortex; t = temporal cortex; th = thalamus; tr = postpiriform transition cortex; z = zona incerta. Scale bars = 1mm. (C; i and ii) IHC of serial coronal sections of human medial temporal lobe. Anatomic annotations: e = entorhinal cortex; h = hippocampus; pr = perirhinal cortex; s = subiculum. Upper dashed box indicates region shown in subpanels iii and iv. Lower right dashed rectangle indicates region shown in subpanels v and vi. Scale bars = 2mm. (iii and iv) IHC of TRIM9 and TRIM67 in the entorhinal cortex (e). Scale bars = 200 μ m. Throughout the figure, black arrows indicate select regions of TRIM9 > TRIM67 immunoreactivity, and white arrows indicate select regions of TRIM67 > TRIM9 immunoreactivity. (v and vi) IHC of TRIM9 and TRIM67 in serial sections of the human hippocampal formation. Anatomic annotations: a = alveus; pl = polyform layer/hilus; sg = stratum granulare; slm = stratum lacunosum moleculare; so = stratum oriens; sp = stratum pyramidale; sr = stratum radiatum. Scale bars = 250 μ m. f = fornix, fg = frontal gyrus, wm = white matter [Color figure can be viewed at www.annalsofneurology.org]

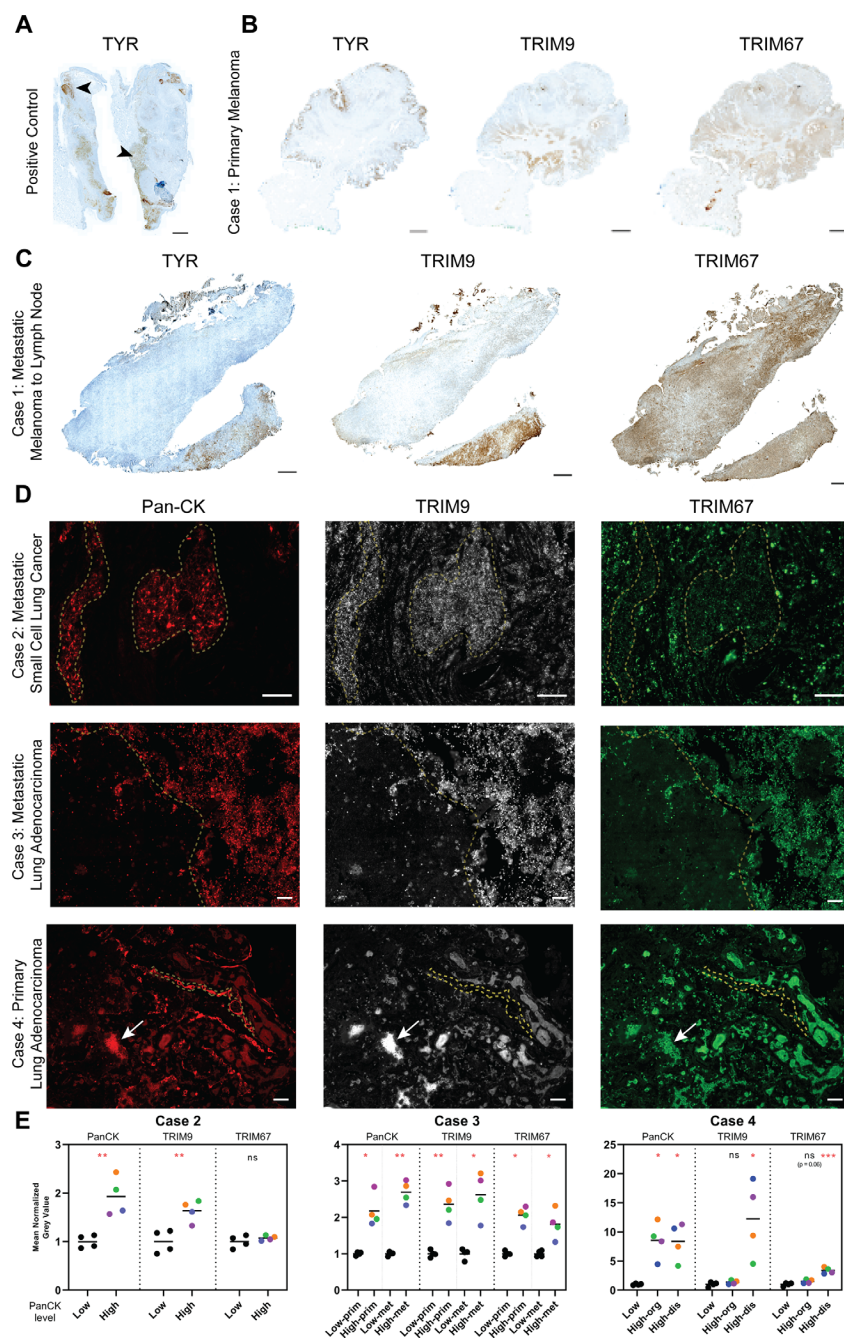


FIGURE 6: Immunohistochemistry of TRIM9 and TRIM67 in patient tumors. (A) Diaminobenzidine (DAB) immunostaining of tyrosinase (TYR) in metastatic melanoma to tonsils as a positive control. Scale bar = 1mm. (B) Serial sections of Case 1 primary melanoma tissue were DAB immunostained for TYR, TRIM9, and TRIM67. Little overlap is observed. Scale bars = 1mm. (C) Serial sections from Case 1 of metastatic melanoma to lymph nodes were DAB immunostained for TYR, TRIM9, and TRIM67. Visually, the intensity of TRIM9 immunostaining is stronger in TYR+ than TYR- regions. In contrast, the intensity of TRIM67 immunostaining is invariant between TYR+ and TYR- regions. Scale bars = 1mm. (D) Multiplex immunofluorescent staining with tumor marker (pancytokeratin [panCK] clone AE1/AE3 (red), anti-TRIM9 (white), and anti-TRIM67 (green). Case 2, top row: panCK+ areas lie within yellow dotted boundaries. Case 3, middle row: the panCK+ area is to the right of the yellow dotted line. Case 4, bottom row: the parallel yellow lines demarcate panCK+ cells that are not anti-TRIM9 and anti-TRIM67 immunoreactive. The arrows point to a cluster of panCK+ cells that are immunoreactive to anti-TRIM9 and anti-TRIM67. Scale bars = 50 μ m. (E) Quantification of the panCK, TRIM9, and TRIM67 immunostaining of tumors shown in D. For each antibody, the mean grey value of 4 panCK^{low} and four panCK^{high} regions of interest (ROIs; orange = ROI 1, green = ROI 2, blue = ROI 3, purple = ROI 4) was measured. Mean grey values were normalized to the mean of the 4 panCK^{low} ROIs. For Case 3, 2 tumor tissues were evaluated: primary (prim) and metastatic (met). For Case 4, mean grey value measurements from cytoarchitecturally organized (org) and disorganized (dis) ROIs were taken from within the same primary tumor tissue. Probability values were calculated using unpaired, 2-tailed *t* tests with Welch correction when appropriate. ns = not significant given a significant threshold of 0.05. **p* \leq 0.05, ***p* \leq 0.01, ****p* \leq 0.001. [Color figure can be viewed at www.annalsofneurology.org]

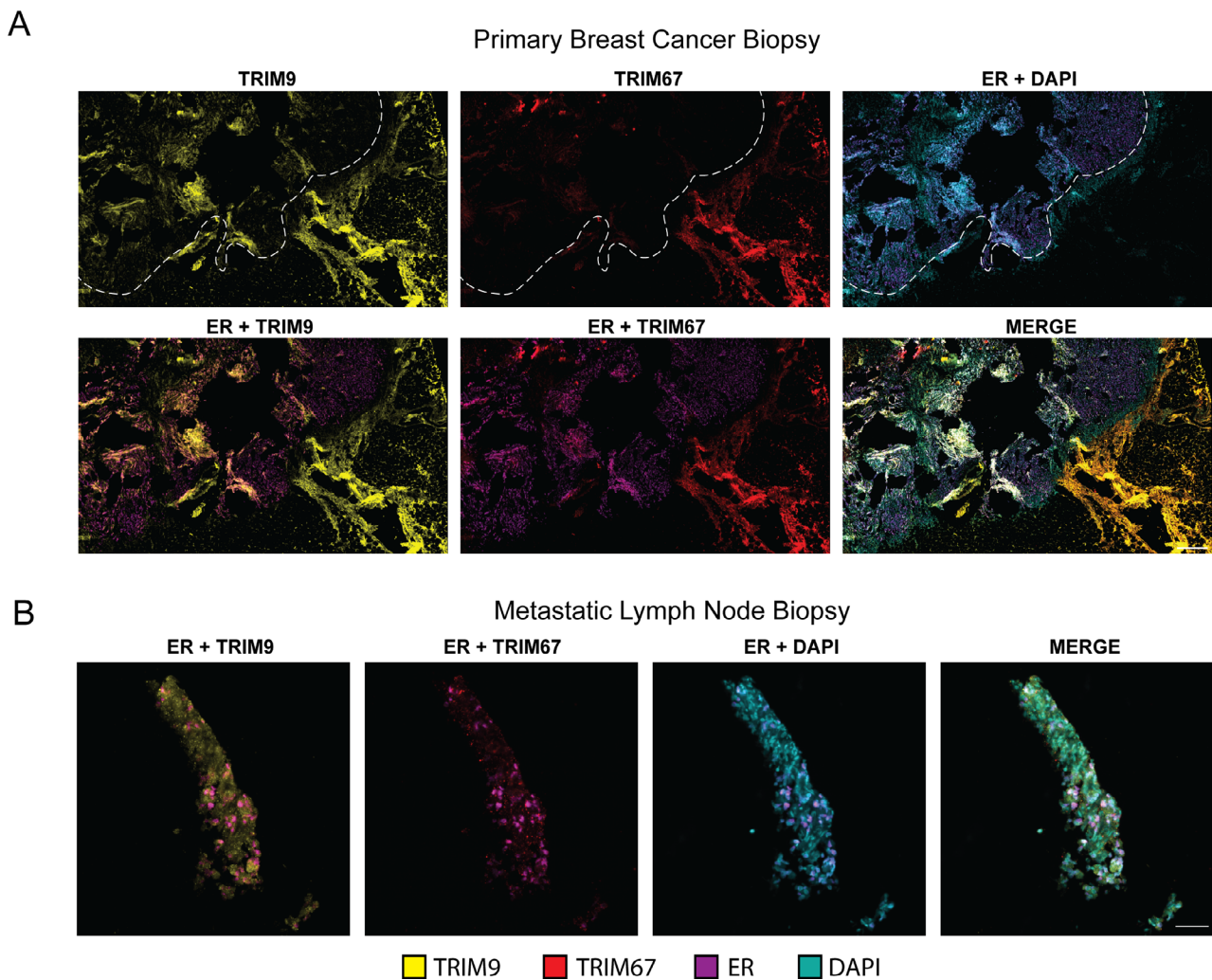


FIGURE 7: TRIM9 and TRIM67 protein expression in Case 5 breast cancer. (A) Multiplex immunofluorescence (mIF) for TRIM9, TRIM67, estrogen receptor (ER), and 4,6-diamidino-2-phenylindole (DAPI) on primary breast cancer tissue. The dotted line indicates the boundary between the ER+ (left) and ER- (right) region of the tissue. Scale bar = 500µm. (B) mIF of metastatic breast cancer to lymph node. Scale bar = 50µm. [Color figure can be viewed at www.annalsofneurology.org]

Like anti-Yo²² and anti-Ri,²³ our TRIM9/67-IgG cerebellar cases uniformly had a mild pleocytosis with elevated protein and generally had normal or nondiagnostic magnetic resonance imaging findings. Like anti-Yo and anti-Ri, most cerebellar cases had poor outcomes characterized by static or progressive symptoms. In no case did immunotherapy reverse or improve cerebellar symptoms. However, in contrast to anti-Yo and anti-Ri, melanoma was associated with 29% of known TRIM9/67-IgG patients with cancer (1 of whom was on an immune checkpoint inhibitor) and 14% of all TRIM9/67-IgG cases. Melanoma-associated paraneoplastic cerebellar syndromes are exceedingly rare, many of which have been reported without an identified autoantibody.^{24–29} Seropositive melanoma-associated paraneoplastic cerebellar cases include SEPTIN3³⁰ (n = 2), Yo³¹ (n = 1), GABABR³² (n = 1), CARP-VIII³³ (n = 1), ARHGAP26³⁴ (n = 1), and an anti-TRIM9/67-IgG case (n = 1).³

This study highlights some additional benefits of complementing traditional autoantibody discovery and validation methods with PhIP-Seq. As demonstrated here, PhIP-Seq epitope mapping aids direct comparison of paraneoplastic polyclonal antibody responses to paralogous gene pairs like TRIM9/TRIM67; as was also done for CDR2L/CDR2 in anti-Yo paraneoplastic cerebellar degeneration.^{4,35} PhIP-Seq may be particularly well suited to identify autoantibodies elicited by cancer-associated neoantigens, even against a background of systemic autoimmunity.³⁶ As a massively parallel antibody detection method, PhIP-Seq may also aid in identifying autoimmune neurological patients who harbor additional antibodies that may contribute to illness presentation.³⁷ Moreover, PhIP-Seq has detected autoantibodies that fail to bind rodent brain tissue³⁵ or novel autoantibodies that do not recognize a rodent ortholog,³⁸ or for which a rodent ortholog does not exist.³⁹ However, the sensitivity of PhIP-Seq is hampered by the absence of post-

translational modifications and limited conformational representation.

Although PhIP-Seq identified the homologous TRIM9/TRIM67 B-box 2 domains as immunodominant peptide epitopes, not all cases were immunoreactive to this epitope. That some cases recognize TRIM9/67 by IP-MS and CBA but not PhIP-Seq or immunoblot indicates the presence of conformational epitope-dependent TRIM9 and TRIM67 autoantibodies and likely explains the superior sensitivity of CBA, which should inform future diagnostic test design. CBA is also a specific test for TRIM9/67-IgG neurologic autoimmunity. We previously demonstrated that TRIM9/67-IgG was not detected in sera of SCLC patients with a paraneoplastic syndrome ($n = 63$), sera from lung adenocarcinoma patients with PNS ($n = 36$), CSF from patients with autoimmune encephalitis ($n = 100$), or CSF from neurodegenerative disease patients ($n = 165$).¹ Furthermore, we did not detect enrichment of TRIM9/67 by healthy CSF ($n = 42$) or neuro-inflammatory CSF with and without cancer ($n = 789$) in our PhIP-Seq database. Taken together, these data indicate that TRIM9/67-IgG is a specific marker of neurological autoimmunity, most commonly a paraneoplastic cerebellar syndrome. Notably, TRIM46, another class I TRIM family autoantigen, is also a specific marker of diverse autoimmune neurological presentations.⁴⁰

Although subacute cerebellar syndrome was the dominant TRIM9/67-IgG phenotype, TRIM9/67 antibody-positive encephalitis cases were observed as well. Case 8's presentation was compatible with GAD65 encephalitis. Of note, Case 9 enriched ZIC1, a paraneoplastic cerebellar degeneration biomarker,¹⁶ by PhIP-Seq. Additionally, we did not detect other classified encephalitis autoantibodies in Cases 7 or 9, and both enriched other neural candidate antigens by PhIP-Seq, suggesting that their phenotype may have been driven by another autoantigen. TRIM9-IgG and TRIM67-IgG antibody titers were significantly lower in the CSF and nominally lower in the serum of TRIM9/67-IgG encephalitis compared to cerebellar cases. Additionally, all tested cerebellar syndrome cases recognized TRIM9/67 by immunoblot, whereas encephalitis Cases 7, 8, and 9 and unknown phenotype Case 11 recognized bands other than TRIM9/67. Although extracerebellar features have been observed in other paraneoplastic PCDs, these data suggest that in some cases TRIM9/67-IgG may co-occur in other autoimmune neurological disorders. Nonetheless, because TRIM9/67-IgG is a sensitive and specific marker of neurological autoimmunity, testing may be warranted in seronegative autoimmune encephalitis.

Because both TRIM9^{41,42} and TRIM67⁴³ have been implicated in proliferation and migration of tumor cells, it is

not obvious a priori which might be the primary antigen in paraneoplastic cases. The apparent obligate co-occurrence of TRIM9 and TRIM67 autoantibodies is likely due to antibody cross-reactivity mediated by sequence and structural homology. However, although all cases were positive for both TRIM9 and TRIM67 autoantibodies by CBA, patient IgG colocalized with TRIM9 and not TRIM67 in mouse brain tissue. Nonetheless, TRIM67 has been proposed as the primary antigenic target³ with epitope spreading⁴⁴ to TRIM9, but this has not been experimentally confirmed. Here, we found higher TRIM9 protein expression in cancer versus noncancer cells in cancer biopsies ($n = 4/5$ cases), and documented TRIM9 and TRIM67 protein expression in a fifth case with primary breast cancer. In contrast, TRIM67 protein was highly expressed in cancer biopsies from only 2 of the same 5 patients. These data suggest that in some cases TRIM9 is the antigenic initiator of TRIM9/67 paraneoplastic autoimmunity.

Overall, these studies indicate that TRIM9/67-IgG are high-risk paraneoplastic biomarkers for which CBA is likely the most sensitive assay. Although TRIM9/67-IgG cases were less common than anti-Yo and anti-Ri at 2 testing sites, systematic testing is required to establish its true prevalence. Future studies of the pathobiology of TRIM9/67-IgG syndromes should include human leukocyte antigen typing with T-cell stimulation assays, comparative genomics of tumors from TRIM9/67-IgG positive and negative patients,⁴⁵ and neuropathological characterizations.

Limitations

Of cases with evidence of TRIM9/67 autoimmunity by 2 methods, CBA was estimated to be 100% sensitive. However, this may be an overestimate due to the limited number of TRIM9/67 cases in this study. Although we report a new association between TRIM9/67-IgG and encephalitis, additional cases are required to determine whether TRIM9/67-IgG is a bystander in autoimmune encephalitis. Our commercial TRIM9 antibody demonstrated cross-reactivity with TRIM67 by CBA but did not overlap with TRIM67 immunostaining in tissue. Nonetheless, we cannot entirely exclude that some tissue TRIM9 signal is due to TRIM67 cross-reactivity. Furthermore, although our commercial TRIM67 antibody did not recognize TRIM9, we cannot rule out that it binds to other off-target proteins. PhIP-Seq indicated a more diverse antibody response to TRIM9 than TRIM67 across the cohort. However, the difference in diversity may be due to inherent biases in the composition of the phage library. Finally, our human brain TRIM9 and TRIM67 staining was limited to a single donor; therefore, these findings may not generalize.

Acknowledgments

This work was supported by NIH National Institute of Mental Health R01MH122471 (S.J.Pl., M.R.W., K.C.Z., J.L.D.) and R25MH060482 (C.M.B.), NIH National Institute of Neurological Disorders and Stroke K08NS096117 (M.R.W.), Brain Research Foundation (S.J. Pl.), Westridge Foundation (M.R.W.), National Multiple Sclerosis Society Clinician Scientist Development Award FAN-1608-25607 (R.D.S.), and the John A. Watson Scholar Program, UCSF (C.M.B., M.T.). M.D.G. was supported by NIH/National Institute on Aging (NIA) R01 AG031189, NIH/NIA R01 AG062562, and the Michael J. Homer Family Fund. J.L.D. is additionally supported by the Chan Zuckerberg Biohub. C.M.B. is additionally supported by a Hanna H. Gray Fellowship, Howard Hughes Medical Institute, a President's Postdoctoral Fellowship Program, the University of California, and a Deeda Blair Research Initiative for Disorders of the Brain. This study is supported by Fondation pour la recherche médicale (FRM-DQ20170336751). This work has been developed within the BETPSY project, which is supported by a public grant overseen by the Agence Nationale de la Recherche (ANR) as part of the second Investissements d'Avenir program (ANR-18-RHUS-0012) and has been performed within the framework of the LABEX CORTEX (ANR-11-LABX-0042) of Université de Lyon operated by the ANR. Confocal microscopy with the CSU-W1 spinning disk was supported by the S10 Shared Instrumentation grant (1S10OD017993-01A1). This work was further supported by the UCSF Histology & Biomarker Core; a subgroup of the Helen Diller Family Comprehensive Cancer Center Biorepository and Tissue Biomarker Technology Core (BTBMT). The BTBMT is supported by the National Cancer Institute under award number P30CA082103.

We thank the patients and families for participation in this study; the Center of MS and Autoimmune Neurology at Mayo Clinic for patient specimen collection funding and research support; the Rocky Mountain MS Center and the Drake family in support of the Autoimmune and Paraneoplastic Neurological Disease Registry at the University of Colorado; Dr S. Gupton for advice; Drs D. Larsen, K. Herrington, and S. Kim of the University of California, San Francisco Nikon Imaging Center for their imaging support; and J. Weinger, E. Tran, and H. Sample for assistance with participant consents. Sequencing was performed at the UCSF Center for Advanced Technology, supported by UCSF Sandler Program for Breakthrough Biomedical Research, Research Resource Program Institutional Matching Instrumentation Award, and NIH 1S10OD028511-01 grants. Molecular graphics and analyses

were performed with UCSF ChimeraX, developed by the Resource for Biocomputing, Visualization, and Informatics at UCSF, with support from NIH R01-GM129325 and the Office of Cyber Infrastructure and Computational Biology, National Institute of Allergy and Infectious Diseases. Human tissue samples were provided by the Neurodegenerative Disease Brain Bank at the University of California, San Francisco, which receives funding support from NIH grants P01AG019724 and P50AG023501, the Consortium for Frontotemporal Dementia Research, and the Tau Consortium. L.D.D., S.M.-C., A.-L.P., and J.H. thank NeuroBioTec Hospices Civils de Lyon Biological Research Center (France, AC-2013-1867, NFS96-900) for banking sera and CSF samples.

Author Contributions

C.M.B., J.H., T.T.N., M.R.W., and S.J.Pl. contributed to conception and design of the study. A.L.P., A.-L.P., A.F.K., A.T., A.Z., B.D.A., B.Y., C.M.B., J.H., J.L.D., J.M.G., K.C.Z., D.L.D., M.D.G., M.R.W., M.P.S., P.W.H., R.D., R.D.S., S.M.-C., T.T.N., and W.D.B. contributed to acquisition and analysis of data. A.Z., C.M.B., J.H., J.M.G., D.L.D., M.D.G., M.P.S., M.R.W., M.T., P.W.H., S.J.Pi., and T.T.N. contributed to drafting the text and/or preparing the figures. S.A.M. and M.M. contributed to acquisition of data.

Potential Conflicts of Interest

A.L.P. reports grant and research support from Genentech; and consulting fees from Alexion, Genentech/Roche, UCB, and EMD Sorono. M.R.W. has received research support from Roche/Genentech and Novartis as well as speaking honoraria from Novartis, Takeda, and Genentech, companies that make therapeutics that could be relevant to paraneoplastic disease. S.J.Pi. and A.Z. work as consultants in the Mayo Clinic Neuroimmunology Laboratory clinical service that commercially offers neural autoantibody testing, but revenue accrued does not contribute to salary, research support, or personal income for any of the authors. J.H. and D.L.D. have filed for a patent (PCT/EP/2019/061280) to protect biological tests to detect anti-TRIM9/67 autoantibodies in patients. All other authors have nothing to report.

Data Availability

Raw data were generated at University of California, San Francisco and Universités de Lyon. Derived data supporting the findings of this study are available from the corresponding authors on request.

References

- Do LD, Gupton SL, Tanji K, et al. TRIM9 and TRIM67 are new targets in paraneoplastic cerebellar degeneration. *Cerebellum* 2019;18:245–254. <https://doi.org/10.1007/s12311-018-0987-5>.
- Sebbag E, Psimaras D, Baloglu S, et al. Immune-related cerebellar ataxia: a rare adverse effect of checkpoint inhibitor therapy. *J Neuroimmune Pharmacol* 2021;17:377–379. <https://doi.org/10.1007/s11481-021-10026-3>.
- Larman HB, Zhao Z, Laserson U, et al. Autoantigen discovery with a synthetic human peptidome. *Nat Biotechnol* 2011;29:535–541. <https://doi.org/10.1038/nbt.1856>.
- O'Donovan B, Mandel-Brehm C, Vazquez SE, et al. High-resolution epitope mapping of anti-Hu and anti-Yo autoimmunity by programmable phage display. *Brain Commun* 2020;2:fcaa059. <https://doi.org/10.1093/braincomms/fcaa059>.
- Short KM, Cox TC. Subclassification of the RBCC/TRIM superfamily reveals a novel motif necessary for microtubule binding. *J Biol Chem* 2006;281:8970–8980. <https://doi.org/10.1074/jbc.M512755200>.
- Tanji K, Kamitani T, Mori F, et al. TRIM9, a novel brain-specific E3 ubiquitin ligase, is repressed in the brain of Parkinson's disease and dementia with Lewy bodies. *Neurobiol Dis* 2010;38:210–218. <https://doi.org/10.1016/j.nbd.2010.01.007>.
- Winkle CC, McClain LM, Valtschanoff JG, et al. A novel Netrin-1-sensitive mechanism promotes local SNARE-mediated exocytosis during axon branching. *J Cell Biol* 2014;205:217–232. <https://doi.org/10.1083/jcb.201311003>.
- Kozareva V, Martin C, Osorno T, et al. A transcriptomic atlas of mouse cerebellar cortex comprehensively defines cell types. *Nature* 2021;598:214–219. <https://doi.org/10.1038/s41586-021-03220-z>.
- Boyer NP, Monkiewicz C, Menon S, et al. Mammalian TRIM67 functions in brain development and behavior. *eNeuro* 2018;5:ENEURO.0186-18.2018. <https://doi.org/10.1523/eneuro.0186-18.2018>.
- Song E, Bartley CM, Chow RD, et al. Divergent and self-reactive immune responses in the CNS of COVID-19 patients with neurological symptoms. *Cell Rep Med* 2021;2:100288. <https://doi.org/10.1016/j.xcrm.2021.100288>.
- Zekeridou A, Kryzer T, Guo Y, et al. Phosphodiesterase 10A IgG: a novel biomarker of paraneoplastic neurologic autoimmunity. *Neurology* 2019;93:e815–e822. <https://doi.org/10.1212/wnl.0000000000007971>.
- Graus F, Titulaer MJ, Balu R, et al. A clinical approach to diagnosis of autoimmune encephalitis. *Lancet Neurol* 2016;15:391–404. [https://doi.org/10.1016/s1474-4422\(15\)00401-9](https://doi.org/10.1016/s1474-4422(15)00401-9).
- Sjöstedt E, Zhong W, Fagerberg L, et al. An atlas of the protein-coding genes in the human, pig, and mouse brain. *Science* 2020;367:eaay5947. <https://doi.org/10.1126/science.aay5947>.
- Deutscher S. Phage display to detect and identify autoantibodies in disease. *N Engl J Med* 2019;381:89–91. <https://doi.org/10.1056/NEJMcibr1903249>.
- Bartley CM, Johns C, Ngo TT, et al. Anti-SARS-CoV-2 and autoantibody profiles in the cerebrospinal fluid of 3 teenaged patients with COVID-19 and subacute neuropsychiatric symptoms. *JAMA Neurol* 2021;78:1503–1509. <https://doi.org/10.1001/jamaneurol.2021.3821>.
- Sabater L, Bataller L, Suárez-Calvet M, et al. ZIC antibodies in paraneoplastic cerebellar degeneration and small cell lung cancer. *J Neuroimmunol* 2008;201-202:163–165. <https://doi.org/10.1016/j.jneuroim.2008.01.018>.
- Matsuura K, Kobayashi S, Konno K, et al. SIPA1L1/SPAR1 interacts with the Neurabin family of proteins and is involved in GPCR signaling. *J Neurosci* 2022;42:2448–2473. <https://doi.org/10.1523/jneurosci.0569-21.2022>.
- Li C, Zhang J, Yang X, et al. hsa_circ_0003222 accelerates stemness and progression of non-small cell lung cancer by sponging miR-527. *Cell Death Dis* 2021;12:807. <https://doi.org/10.1038/s41419-021-04095-8>.
- Yaguchi H, Okumura F, Takahashi H, et al. TRIM67 protein negatively regulates Ras activity through degradation of 80K-H and induces neuritogenesis. *J Biol Chem* 2012;287:12050–12059. <https://doi.org/10.1074/jbc.M111.307678>.
- Muñiz-Castrillo S, Vogrig A, Ciano-Petersen NL, et al. Novelty in autoimmune and paraneoplastic cerebellar ataxias: twenty years of progresses. *Cerebellum* 2022;21:573–591. <https://doi.org/10.1007/s12311-021-01363-3>.
- Graus F, Vogrig A, Muñiz-Castrillo S, et al. Updated diagnostic criteria for paraneoplastic neurologic syndromes. *Neurology* 2021;8:e1014. <https://doi.org/10.1212/wni.000000000001014>.
- Venkatraman A, Opal P. Paraneoplastic cerebellar degeneration with anti-Yo antibodies—a review. *Ann Clin Transl Neurol* 2016;3:655–663. <https://doi.org/10.1002/acn3.328>.
- Luque FA, Furmeaux HM, Ferziger R, et al. Anti-Ri: an antibody associated with paraneoplastic opsoclonus and breast cancer. *Ann Neurol* 1991;29:241–251. <https://doi.org/10.1002/ana.410290303>.
- Berger JR, Mehari E. Paraneoplastic opsoclonus-myoclonus secondary to malignant melanoma. *J Neurooncol* 1999;41:43–45. <https://doi.org/10.1023/a:1006189210197>.
- Jung KY, Youn J, Chung CS. Opsoclonus–myoclonus syndrome in an adult with malignant melanoma. *J Neurol* 2006;253:942–943. <https://doi.org/10.1007/s00415-006-0026-1>.
- Hauspy J, Nevin A, Harley I, et al. Paraneoplastic syndrome in vaginal melanoma: a case report and review of the literature. *Int J Gynecol Cancer* 2007;17:1159–1163. <https://doi.org/10.1111/j.1525-1438.2006.00857.x>.
- Dresco F, Aubin F, Deveza E, et al. Paraneoplastic Opsoclonus-myoclonus syndrome preceding a mucosal malignant melanoma. *Acta Derm Venereol* 2019;99:337–338. <https://doi.org/10.2340/00015555-3062>.
- Jiménez-Zarazúa O, Vélez-Ramírez LN, Alcocer-León M, et al. Paraneoplastic cerebellar degeneration secondary to BRAF mutant melanoma metastasis from an occult primary cancer. *Case Rep Oncol* 2020;13:633–642. <https://doi.org/10.1159/000507729>.
- Mondragón JD, Jiménez-Zarazúa O, Vélez-Ramírez LN, et al. Paraneoplastic opsoclonus-myoclonus syndrome secondary to melanoma metastasis from occult primary cancer. *Case Rep Neurol* 2019;11:66–79. <https://doi.org/10.1159/000497034>.
- Miske R, Scharf M, Borowski K, et al. Septin-3 autoimmunity in patients with paraneoplastic cerebellar ataxia. *J Neuroinflammation* 2023;20:88. <https://doi.org/10.1186/s12974-023-02718-9>.
- Valpione S, Zoccarato M, Parrozzani R, et al. Paraneoplastic cerebellar degeneration with anti-Yo antibodies associated with metastatic uveal melanoma. *J Neurol Sci* 2013;335:210–212. <https://doi.org/10.1016/j.jns.2013.08.026>.
- Jarius S, Steinmeyer F, Knobel A, et al. GABAB receptor antibodies in paraneoplastic cerebellar ataxia. *J Neuroimmunol* 2013;256:94–96. <https://doi.org/10.1016/j.jneuroim.2012.12.006>.
- Bataller L, Sabater L, Saiz A, et al. Carbonic anhydrase-related protein VIII: autoantigen in paraneoplastic cerebellar degeneration. *Ann Neurol* 2004;56:575–579. <https://doi.org/10.1002/ana.20238>.
- Wallwitz U, Brock S, Schunck A, et al. From dizziness to severe ataxia and dysarthria: new cases of anti-Ca/ARHGAP26 autoantibody-associated cerebellar ataxia suggest a broad clinical spectrum. *J Neuroimmunol* 2017;309:77–81. <https://doi.org/10.1016/j.jneuroim.2017.05.011>.
- Bartley CM, Parikshak NN, Ngo TT, et al. Case report: a false negative case of anti-Yo paraneoplastic myelopathy. *Front Neurol* 2021;12:728700. <https://doi.org/10.3389/fneur.2021.728700>.
- Xu GJ, Shah AA, Li MZ, et al. Systematic autoantigen analysis identifies a distinct subtype of scleroderma with coincident cancer. *Proc Natl Acad Sci U S A* 2016;113:E7526–e7534. <https://doi.org/10.1073/pnas.1615990113>.

37. Martinez-Hernandez E, Guasp M, García-Serra A, et al. Clinical significance of anti-NMDAR concurrent with glial or neuronal surface antibodies. *Neurology* 2020;94:e2302–e2310. <https://doi.org/10.1212/WNL.0000000000009239>.
38. Bartley CM, Ngo TT, Cadwell CR, et al. Dual ankyrinG and subpial autoantibodies in a man with well-controlled HIV infection with steroid-responsive meningoencephalitis: a case report. *Front Neurol* 2022;13:1102484. <https://doi.org/10.3389/fneur.2022.1102484>.
39. Mandel-Brehm C, Benson LA, Tran B, et al. ZSCAN1 autoantibodies are associated with pediatric paraneoplastic ROHHAD. *Ann Neurol* 2022;92:279–291. <https://doi.org/10.1002/ana.26380>.
40. Valencia-Sanchez C, Knight AM, Hammami MB, et al. Characterisation of TRIM46 autoantibody-associated paraneoplastic neurological syndrome. *J Neurol Neurosurg Psychiatry* 2022;93:196–200. <https://doi.org/10.1136/jnnp-2021-326656>.
41. Wang X, Shu Y, Shi H, et al. TRIM9 is up-regulated in human lung cancer and involved in cell proliferation and apoptosis. *Int J Clin Exp Med* 2016;9:10461–10469.
42. Yang F, Liu H, Yu Y, Xu L. TRIM9 overexpression promotes uterine leiomyoma cell proliferation and inhibits cell apoptosis via NF- κ B signaling pathway. *Life Sci* 2020;257:118101.
43. Jiang J, Ren H, Xu Y, et al. TRIM67 promotes the proliferation, migration, and invasion of non-Small-cell lung cancer by positively regulating the notch pathway. *J Cancer* 2020;11:1240–1249. <https://doi.org/10.7150/jca.38286>.
44. Powell AM, Black MM. Epitope spreading: protection from pathogens, but propagation of autoimmunity? *Clin Exp Dermatol* 2001;26:427–433. <https://doi.org/10.1046/j.1365-2230.2001.00852.x>.
45. Small M, Treilleux I, Couillault C, et al. Genetic alterations and tumor immune attack in Yo paraneoplastic cerebellar degeneration. *Acta Neuropathol* 2018;135:569–579. <https://doi.org/10.1007/s00401-017-1802-y>.